Functionalized Thiophosphate and Oxidic Filler Particles for Hybrid Solid Electrolytes

Laura Helmers,*[a] Finn Frankenberg,[a] Julian Brokmann,[a] Christine Burmeister,[a] Annika Buchheit,[b] Arno Kwade,[a] and Peter Michalowski[a]

To achieve the commercialization of solid-state-batteries (SSBs), solid electrolyte properties need to be further improved. The hybrid solid electrolyte (HSE) approach is expected to combine the favorable properties of different solid electrolyte classes and is therefore systematically investigated. Mixing low amounts of thiophosphate or oxide filler particles (FP) into a polyethylene oxide (PEO) polyethylene glycol (PEG) and lithium salt bis(trifluoromethane)sulfonimide (LiTFSI) matrix cannot improve the electrochemical properties. Silanization of the thiophosphate FPs significantly increases the ionic conductivity to 0.1 mS cm^{-1} at room temperature compared to 0.017 mS cm^{-1} for a pure PEO solid electrolyte. Moreover, a correlation between the intrinsic conductivity of the FPs and the resulting conductivity of the HSE is observed. Also, the functionalization is successfully transferred to oxide FPs. In addition to an equally significant increase in ionic conductivity, a strong influence of the crystallite size of the FPs on the resulting ionic conductivity of the HSE was found. The discovered effect of FP surface structure on overall HSE conductivity indicates a participation of the FP surface in ion transport and emphasizes the need for tailored filler design in HSE applications.

Introduction

Lithium-ion batteries (LIB) are the commonly used technology in electronic devices like Smartphones and Laptops as well as electric vehicles. Although substantial progress has been made over the last decades, conventional Lithium-ion batteries (LIBs) still suffer from safety issues due to the use of a highly flammable and poisonous liquid electrolyte.[1] Along with it, the common technology is nearly at its limit of progress which hinders the further increase in the range of an electric vehicle (EV).[2] To raise the acceptance for the use in electric vehicles and to expedite the energy transition to more renewable energy, a safer technology offering the potential to reach higher performance is needed.

To achieve this, the use of a lithium-metal anode has been suggested due to its low electrochemical potential (−3.04 V) and the high theoretical capacity (3860 mAh g^{-1}), enabling the application of thin anodes.[3] In conventional LIB this is inhibited by dendrite formation leading to failures up to explosion.[1] All-solid-state batteries (ASSB) provide the opportunity to overcome this issue by the use of a mechanically stable solid electrolyte (SE) and thereby a significant increase in the attainable energy density as well as improved safety.[3]

Solid electrolytes can be separated into two major classes: organic and inorganic. Organic electrolytes like Poly (ethylene oxide) (PEO) provide a good interfacial contact to the electrodes, are easy to process and stable against a lithium-metal anode.[4] Besides, PEO is light in weight and cheap which is favorable in view of scale-up and the application in electric vehicles.[4] However, these materials suffer from low ionic conductivities (< 0.02 mS cm^{-1}[5,6]) at room temperature (RT) and a low lithium transference number of 0.18 at 80 °C.[7] Hence, materials like PEO can only be used at elevated temperature. Inorganic electrolytes can be further divided into thiophosphates and oxides. Oxides like lithium lanthanum zirconium oxide (LLZO) show high ionic conductivities (0.2 mS cm^{-1} at RT[8]) but require a sintering step (> 900 °C[9]), associated with high energy costs and possible chemical instability of oxide materials like LLZO towards the cathode active material.[10] Furthermore, materials like LLZO are very brittle resulting in difficult fabrication and the formation of dendrites in spawning cracks and along grain boundaries.[11] Another oxide material lithium aluminum titanium phosphate (LATP) shows a lower skeletal density and high grain-core conductivity (6 mS cm^{-1}), but the overall conductivity is limited by high resistance pathways across grain-boundaries.[12] In addition, LATP is not stable against lithium metal, caused by the redox reaction of Ti^{4+} at the anode interface.[13] Thiophosphate SEs such as $Li_{9.54}Si_{1.74}P_{1.44}S_{11.7}Cl_{0.3}$ show high ionic conductivities up to 25 mS cm^{-1} at RT[14] and a lithium transference number of 1. However, some thiophosphate materials are not stable against the lithium anode.[10] Further a sufficient contact in between the

[a] L. Helmers, F. Frankenberg, J. Brokmann, Dr. C. Burmeister, Prof. A. Kwade, Dr. P. Michalowski
TU Braunschweig
Institute for Particle Technology
38104 Braunschweig (Germany)
E-mail: laura.helmers@tu-braunschweig.de

[b] A. Buchheit
Forschungszentrum Jülich GmbH
Institute of Energy and Climate Research (IEK)
IEK-12: Helmholtz-Institute Münster (HI MS) Ionics in Energy Storage
Corrensstraße 46, 48149 Münster (Germany)

Supporting information for this article is available on the WWW under https://doi.org/10.1002/celc.202300310

thiophosphate particles as well as to the cathode active material particles is challenging, requiring high pressures of 370 MPa[15] which is problematic considering scale-up. Next to that, the possibility of H_2S formation after exposure to atmosphere hinders a large scale production.[16]

To overcome the drawbacks of single organic and inorganic electrolytes, a third class of solid membranes, so-called hybrid solid electrolytes (HSE), is believed to merge the advantages of each class. By incorporating filler particles into the polymer matrix ($w_{Polymer} > 50\%$) or by adding a polymer to inorganic electrolytes ($w_{Polymer} < 50\%$) the ionic conductivity and lithium transference number are expected to increase. For example, by adding 3 wt.-% PEO to $Li_7P_3S_{11}$ (LPS), Xu et al. were able to raise the ionic conductivity from 1.4 to 2.1 mS cm^{-1}.[17] However, due to the high LPS content the challenge of H_2S formation still remains. Wang et al. studied the approach to manufacture lithium lanthanum titanate (LLTO) fibers, which were coated with a PEO electrolyte. For a fiber content of 20 wt.-% LLTO an ionic conductivity of 0.5 mS cm^{-1} was achieved at RT, but due to the difficult fabrication of ceramic fibers high processing costs are to be expected.[18] On the other hand, by mixing 2 wt.-% Li_3PS_4 particles into a PEO matrix Chen et al. could increase the ionic conductivity up to 0.035 mS cm^{-1} at 60 °C.[19] Likewise, Li et al. observed a reduced ionic resistance by the incorporation of active ceramic filler material (LSPS) in a PEO matrix.[20] Further the importance of a homogenous distribution of the filler material was outlined as the ionic resistance increased for agglomerated filler particles. The inhomogeneous distribution leads to unstable voltage, poor rate capability, lower capacity and varying mechanical properties.[21,22] To overcome this problem, a sufficient dispersion and wetting of the filler particles is necessary. Huo et al. studied the wetting of lithium lanthanum tantalum zirconate (LLZTO) filler particles with an ionic liquid leading to an improved ionic conductivity of 0.22 mS cm^{-1} at RT. Even higher ionic conductivities were obtained with a method presented by Pan et al. using chemical binding of the filler particles through silanization in order to reduce the interface resistance.[23] By incorporation of 3 wt.-% $Li_{10}GeP_2S_{12}$ (LGPS) into a PEO matrix an ionic conductivity of almost 1 mS cm^{-1} at room temperature was achieved. Until now the functionalization of filler particles through silanization is rarely investigated and there is a lack of knowledge regarding the application on different filler types.

In this work, we investigated the incorporation of oxide as well as thiophosphate filler particles into a PEO-LiTFSI matrix. Inspired by the work of Pan et al., a silane functionalization was employed to improve the interface between the filler particles and the PEO matrix providing a fast transition pathway through the composite electrolyte. In contrast to Pan et al., Li_3PS_4 (LPS), L_6PS_5Cl (argyrodite) and $Li_{1.3}Al_{0.3}Ti_{1.7}(PO_4)_3$ (LATP) were used as filler particles and additionally varied in particle size. Moreover, for thiophosphate filler particles the dispersing time and energy input during processing was varied and the effect on the resulting HSE properties were determined. For the oxide filler particles, a transfer of the silanization method was studied and the effect of filler particle size and content investigated. The HSEs were examined regarding filler particle distribution, release of H_2S, stability against lithium as well as the resulting ionic conductivity. Analysis of the electrolyte and its previous solutions indicates that silane functionalization results in stabilized suspensions, improved filler particle distribution in the HSE, and subsequently increased ionic conductivity. Further due to the embedded filler particles, the HSEs exhibits a higher stability against air and lithium metal compared to the single solid electrolytes.

Results and Discussion

Thiophosphate filler particles

First of all, the influence of the preparation time and energy input on the ionic conductivity of thiophosphate HSEs was investigated. The dissolving time of LPS in acetonitrile ACN as well as the rest time after adding PEO-PEG and LiTFSI in the dispersing step were varied and the resulting films were characterized with regard to the ionic conductivity via electrochemical impedance spectroscopy (EIS).

As depicted in Figure 1a, the ionic conductivity is slightly enhanced if the suspension is stored for 24 h after the dispersing step. We attribute this increase in conductivity to the degassing of the suspension as no vacuum could be applied with the device. A significant increase in conductivity is visible if LPS is dissolved in ACN for 24 h prior to the dispersing step with PEO/PEG and LiTFSI. The increase in conductivity can be explained by a ligand formation visible through a colour change of the solution to blue (see Figure S1, Supporting Information). The LPS completely dissolves in the acetonitrile as described in Xu et al.[24] Therefore, for all further experiments the thiophosphate particles were dissolved for 24 h in ACN to ensure sufficient time for the ligand formation. No additional increase, but a slightly reduced conductivity could be observed if the suspension was set to rest for 24 h after the dissolving step. Sedimentation and agglomeration effects of LPS particles are likely responsible for this phenomenon. In addition to the process time, the influence of the stress intensity during the dispersing step was investigated (Figure 1b). Therefore, three processes with increasing stress intensity, namely shaking plate, magnetic stirrer with agitator as well as a dissolver were used and compared regarding the resulting ionic conductivity and residual porosity of the HSEs. With rising stress intensity, the porosity decreases and an improved ionic conductivity is observed as the thiophosphate particles as well as the LiTFSI is distributed more homogeneously in the polymer matrix. This is well in line with the stress intensity effect on the dispersion kinetics.[25] Consequently, the dissolver was used for all further experiments.

Afterwards, the influence of the filler content of thiophosphate particles on the ionic conductivity of the HSE was investigated. Therefore, films with 0 vol.-% up to 2.5 vol.-% LPS content were manufactured and analyzed via EIS.

With rising LPS content the conductivity decreases in contrast to results published by Chen et al. or Li et al.[19,20] These results indicate that the LPS particles work as a barrier for ion

Research Article
doi.org/10.1002/celc.202300310

Chemistry Europe
European Chemical Societies Publishing

a)

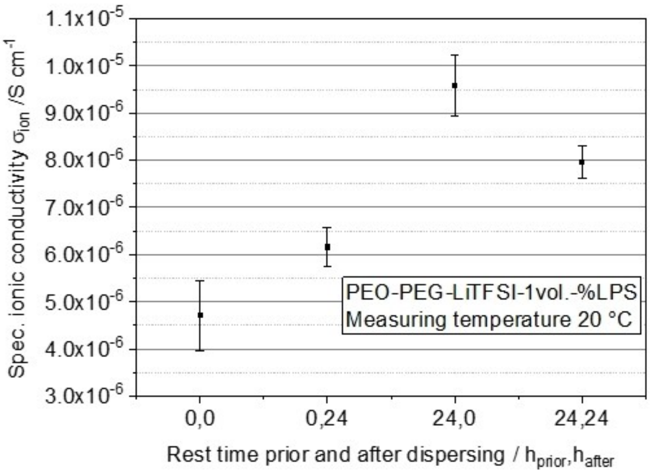

b)

Dispersing device	Porosity ε /%	Ion. conductivity at RT σ_{ion} /S cm^{-1}
Shaking plate	13.84	$4.75 \cdot 10^{-6}$
Magnetic stirrer	12.27	$7.61 \cdot 10^{-6}$
Dissolver	2.34	$1.5 \cdot 10^{-5}$

Figure 1. Ionic conductivity of HSE with 1 vol.-% LPS in dependency of dissolution time prior and after dispersing with a dissolver (a). Ionic conductivity and residual porosity in dependency of the dispersing device for PEO-PEG-LiTFSI-1 vol.-% LPS (b).

transport instead of providing fast transport pathways. Moreover, sedimented material was observed for suspensions with LPS which was analyzed via Raman spectroscopy (Figure 2b). The spectrum shows the typical peaks of pure sulfur, at $\sim 217\ cm^{-1}$ the S–S–S bending and at $\sim 472\ cm^{-1}$ the S–S stretching, indicating that sulfur is precipitated once PEO-PEG and LiTFSI is added.[26] Most likely, the sulfur particles hinder the ion transport (Figure 3a) and decrease the overall ionic conductivity of the HSE. In order to reduce the interface resistance in between filler particles and polymer solid electrolyte (PSE) as well as improving the stability of LPS particles in the HSE, a chemical bonding of the organic and inorganic material was investigated. We presume shortened transport pathways along the interface (2) or even through the filler particles (3) for functionalized LPS particles depicted in Figure 3b.

A silane bonding with (Chloromethyl)(Phenylethyl)Trimethoxys (CTMS) was used to functionalize the LPS particles. The reaction mechanism is illustrated in Figure 4a demonstrating the chemical interaction of CTMS to the LPS surface through a Si–S bond as discovered in Pan et al.[23] According to Zarinwall et al. different types of bonds to the particle surface are possible ranging from single chemical bond up to three chemical bonds or the formation of mono- and multilayers.[27]

To verify the successful functionalization of the LPS particles with CTMS, thermogravimetric analysis (TGA) measurements of pristine and functionalized particles were conducted (Figure 4b). As the mass loss below 200 °C corresponds to physically absorbed water and differs for the samples, the TGA curves are therefore normalized to the value recorded at 200 °C.[28] A significantly increased mass loss of 8.37 % is observed for the functionalized LPS particles compared to pristine LPS particles. This result indicates that the CTMS was successfully grafted via covalent bonding onto the LPS surface.

During subsequent HSE production no sedimented material could be observed for suspensions with functionalized LPS particles. Next to that, the residual porosity is significantly reduced (Figure 2c) for the HSE with 1 vol.-% functionalized LPS from 8.2 % to 0.35 %. As a result, the ionic conductivity at room temperature (RT) increased significantly from $1.4 \cdot 10^{-5}\ S\,cm^{-1}$ for the pure PSE up to $6.2 \cdot 10^{-5}\ S\,cm^{-1}$ for the HSE with 1 vol.-% functionalized LPS (Figure 2d). Furthermore, the transference number of the PEO PSE, PEO-PEG PSE and HSE with functionalized LPS particles was determined to 0.12, 0.52 and 0.55 respectively. Due to the increased transference number, it is likely that the functionalized LPS particles participate in the lithium ion transport. Hence, the covalent bonding of the silane to the particle surface leads to a reduced interface resistance in between the LPS particles and the PSE resulting in faster transport pathways through the solid electrolyte.[23] Scanning electron microscopy (SEM) images of a film with and without silane bonding are shown in Figure 5. The silane does not only effect the LPS interface but also the PSE. For the sample without silane, grain boundaries in between PEG and PEO are visible which are inhibited by the addition of the silane. Moreover, the functionalized LPS particles are more homogeneously distributed. Hence, the addition of silane does not only effect the interface in between the LPS and PSE but also stabilizes the LPS particles within the PEO-PEG matrix and, thus, minimizes agglomeration while inhibiting the formation of sulfur. In order to identify the particle distribution, automatically segmented images are shown in Figure S2, Supporting Information. For the HSE with functionalized filler particles, a significantly lower cluster size and cluster size deviation is observed.

For the processing of LPS-hybrid materials the formation of H_2S plays a crucial role for safety. Therefore, the influence of a chemical bonding and thereby embedding of LPS particles in the PSE phase on the H_2S formation was investigated. The H_2S formation in dependency of exposure time to ambient air is shown in Figure 6a. For the HSE without silane H_2S was formed already during the first 20 min whereas for the HSE with silane functionalization no H_2S could be detected. These results show

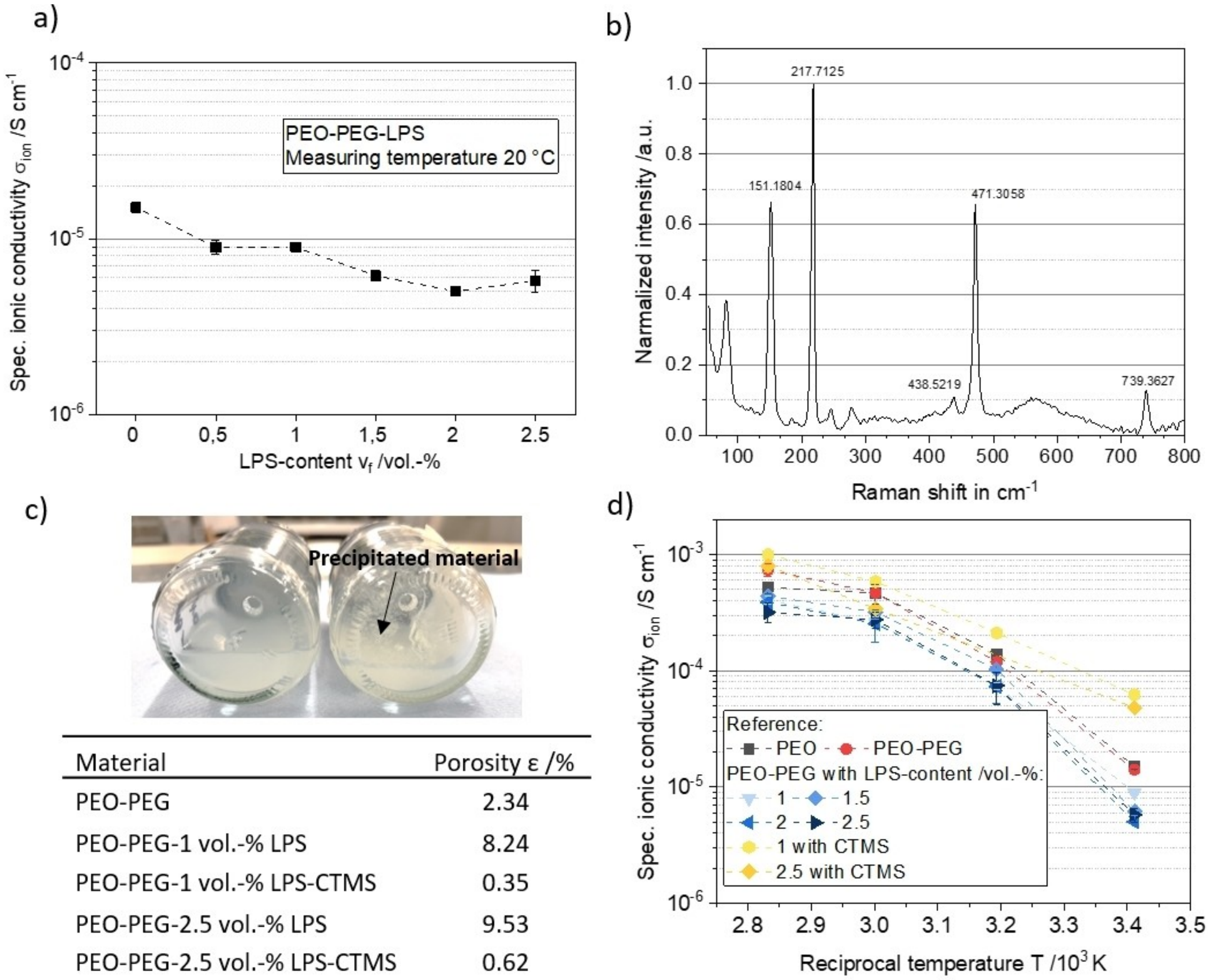

Material	Porosity ε /%
PEO-PEG	2.34
PEO-PEG-1 vol.-% LPS	8.24
PEO-PEG-1 vol.-% LPS-CTMS	0.35
PEO-PEG-2.5 vol.-% LPS	9.53
PEO-PEG-2.5 vol.-% LPS-CTMS	0.62

Figure 2. Specific ionic conductivity as a function of LPS content at 20 °C (a). Raman spectroscopy of sedimented material of the suspension (b), picture of suspension with silane left and without silane right and porosity of HSE with and without silane functionalization (c), specific ionic conductivity of polymer solid electrolyte (PSE) as reference and HSE with different LPS content and with silane functionalization as function of temperature (d).

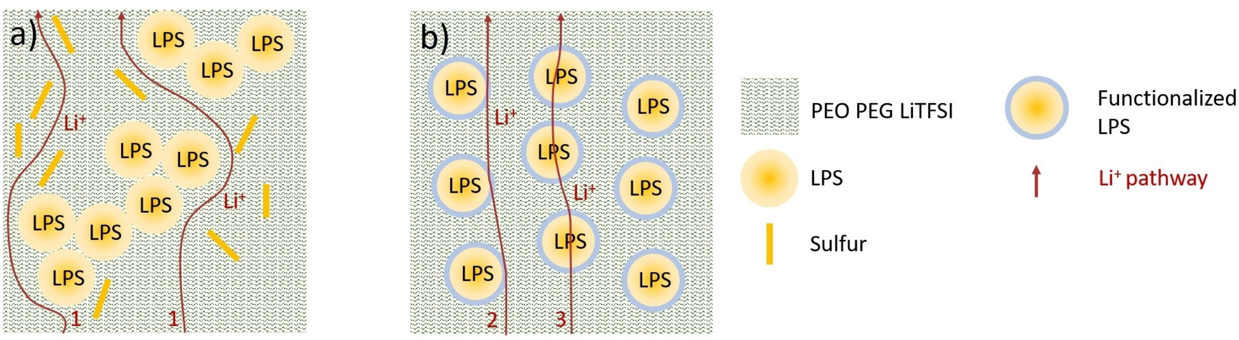

Figure 3. Possible transport pathways through HSE without (a) and with functionalized LPS particles (b).

that the safety of handling the HSE could be significantly improved by a silane bonding. However, as a pure lithium anode should be used to provide high energy densities, an additional challenge is the instability of LPS against lithium. To investigate whether the embedding of LPS particles by the silane functionalization can improve the stability against lithium, the interface resistance was measured via EIS for a symmetric Li-HSE–Li cell with and without silane. As shown in Figure 6b, by silane functionalization the interface resistance is significantly reduced and constant. The HSE with silane shows

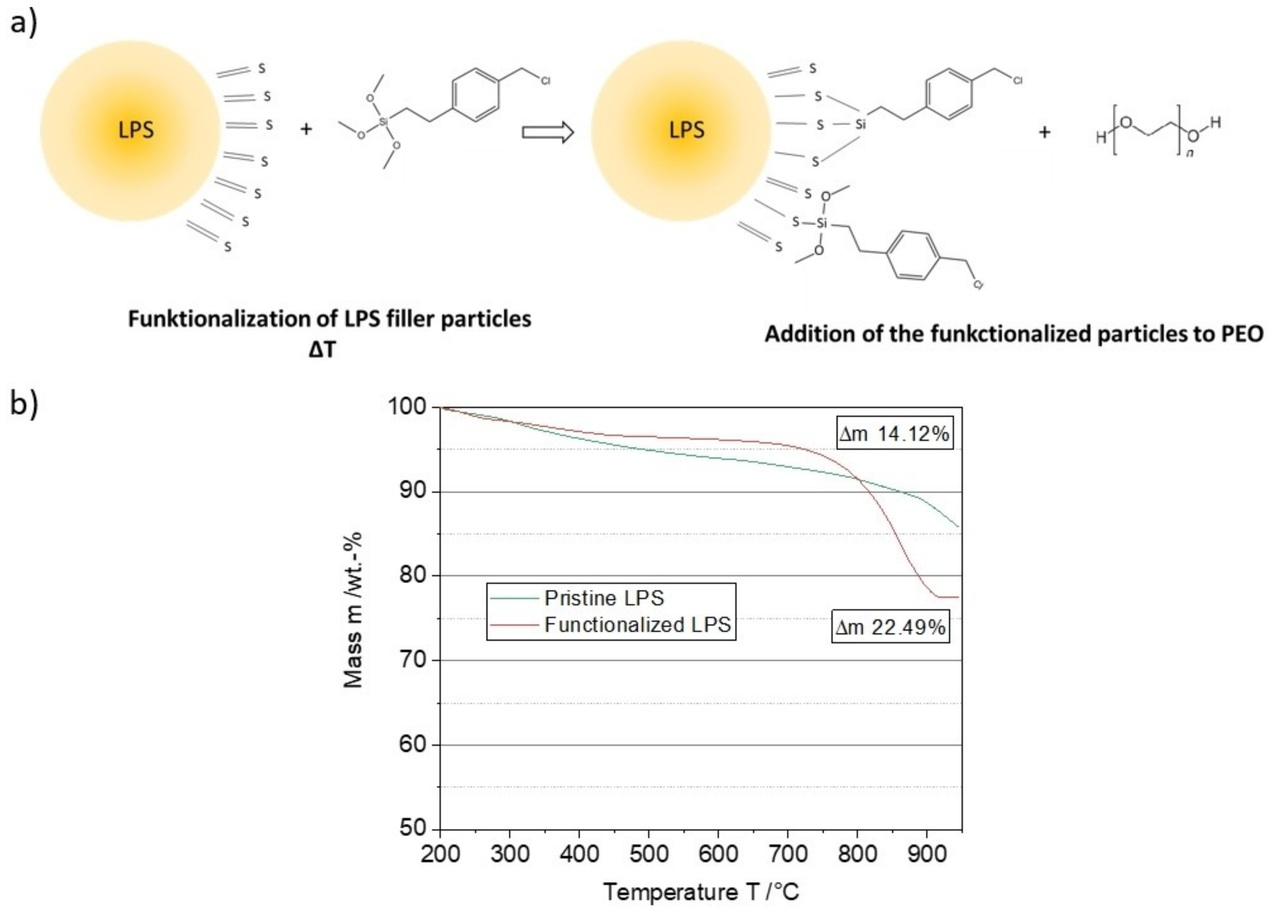

Figure 4. Reaction principle of LPS with CTMS and the addision of functionalized LPS particles to PEO (a), TGA analysis of pristine and functionalized LPS particles (b).

an interface resistance of approx. 60 Ω in contrast to HSE without silane starting at 300 Ω rising up to 500 Ω after a week and 4000 to 5000 Ω after one month. Next to that, for lithium metal symmetric cells a constant voltage is obtained for HSE with functionalized LPS particles, whereas for non-functionalized particles a sharp increase in voltage over time is observed up to 0.5 V. After 190 h the non-functionalized cell exhibits a large voltage drop caused by a short curcuit. The increase in voltage is ascribed to the stability issues if LPS is in direct contact with the lithium metal electrode. After a slight increase in overpotential at the beginning (40 mV) a low polarization voltage (3 mV) is observed for the HSE with functionalized LPS. By functionalization the direct contact of LPS particles with the lithium metal interface is inhibited resulting in an improved cycling stability.

In summary, the ionic conductivity, transference number, suspension stability as well as the chemical stability against lithium and ambient air could be significantly improved by the functionalization of the LPS particles with silane.

Furthermore, the influence of the thiophosphate properties on the ionic conductivity of the HSE was investigated. Therefore, three LPS materials with different intrinsic conductivities and particles sizes as well as an argyrodite material were used as filler material. The thiophosphate properties are shown in the experimental section Table 1. The HSE specific ionic conductivity of PEO-PEG with silane and different thiophosphates as well as the filler particle ionic conductivity is shown in dependency of the thiophosphate type in Figure 6d. Submicron and micron LPS filler particles show a similar HSE ionic conductivity, whereas the HSE ionic conductivity is slightly reduced by amorphous LPS. The highest HSE ionic conductivity was achieved for the argyrodite material with 0.74 $mS\,cm^{-1}$. The comparatively high ionic conductivity for the HSE with argyrodite filler particles indicate that the intrinsic ionic conductivity of the filler particles directly influences the ionic conductivity of the HSE. In addition to the increased transfer number, this observation also implies the involvement of the active filler particles in facilitating the transport of lithium ions. Next to that, the filler particle structure has an impact on the resulting HSE ionic conductivity. The micron-sized amorphous LPS filler particles have a similar particle size to the crystalline LPS particles but exhibit a slightly higher ionic conductivity. Nevertheless, the crystalline filler particles lead to enhanced transport properties in the HSE in comparison to the amorphous LPS filler particles. However, for pure sulfide solid electrolyte (SE) layers, the use of amorphous LPS particles can lead to improved contact between the sulfide particle interfaces, thereby enhancing the overall SE ionic conductivity, despite the higher intrinsic

Research Article
doi.org/10.1002/celc.202300310

Chemistry Europe
European Chemical Societies Publishing

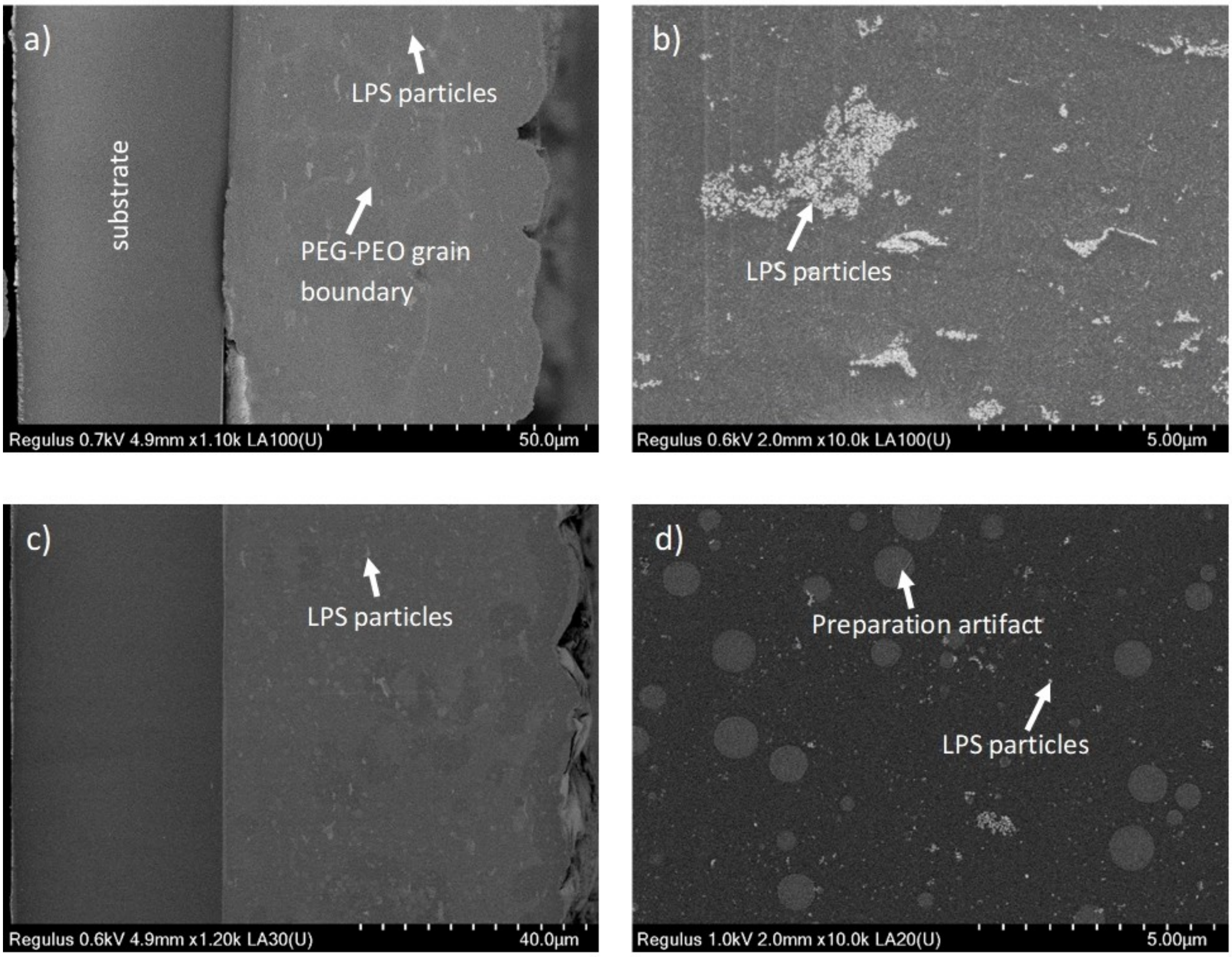

Figure 5. SEM images of HSE with 1 vol.-% LPS in 1.10 k (a) and 10.0 k (b) resolution, HSE with 1 vol.-% LPS and silane functionalization in 1.20 k (c) and 10.0 k (d) resolution.

Table 1. Properties of different filler particles. (*Comparable to values from literature [40] and described in [41], **described in [42]), ***Measured via laser diffraction Figure S9, Supporting information).

Name	Material	Condition	Raw Density ρ/g cm^3	Ion. conductivity σ/mS cm^{-1}	Particle size x_{50}/µm	References
LPS-submicron	β-LPS	cristalline	1.8	0.398**	<1	[42]
LPS-amorphous	LPS	amorphous	1.8	0.33*	8	[41]
LPS-micron	β-LPS	cristalline	1.8	0.259**	8.5	[42]
Argyrodite	Li6PS5Cl	cristalline	1.64	0.87	3	
LATP	$Li_{1.3}Al_{0.3}Ti_{1.7}P_3O_{12}$	–	2.9	0.2–1	1.78***	[39]
LATP grinded	$Li_{1.3}Al_{0.3}Ti_{1.7}P_3O_{12}$	–	2.9	0.2–1	0.085***	[39]
SiLibeads	–	–	2.5	–	2.96	[43]

ionic conductivity of the crystalline LPS phase.[29] These findings suggest that the filler particles' surface plays a role in facilitating lithium ion transport. Therefore, optimizing the LPS material for its application as a filler in HSE demands distinct surface modifications, differing from those required for utilization in purely inorganic solid electrolytes.

For the micron and submicron LPS a similar HSE ionic conductivity is achieved despite the significant differences in particle size. Although the filler particle ionic conductivity is in the same range, we expected significant differences as the use of submicron filler particles can reduce the crystallinity by local changes in the polymer structure and thereby improve the ionic conductivity of the PSE.[30] The submicron particle size should therefore be beneficial, as it also reduces the crystalline phase of the polymer if a homogeneous particle distribution is reached. However, an increased HSE ionic conductivity by the

Research Article
doi.org/10.1002/celc.202300310

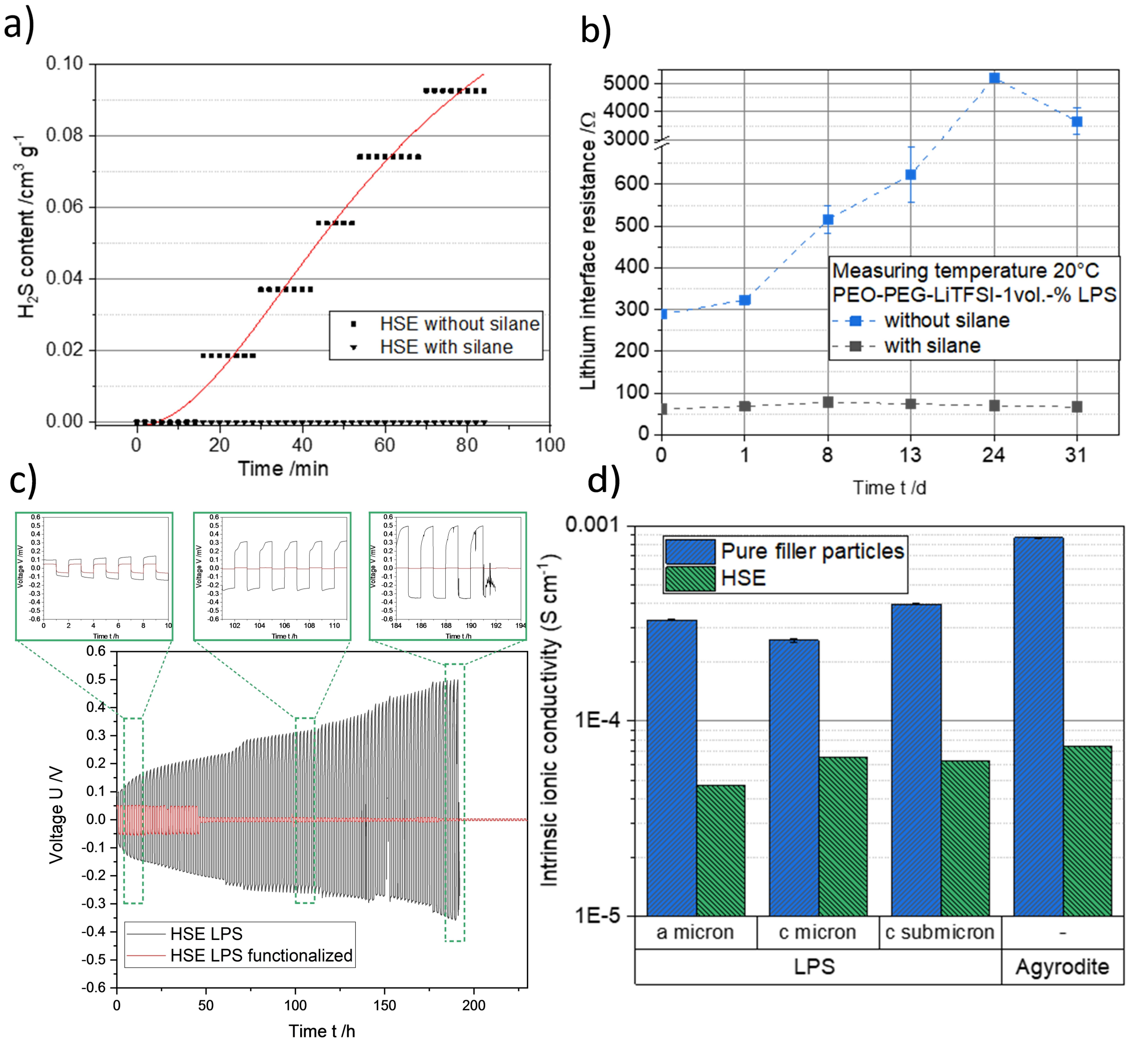

Figure 6. , H_2S formation in dependency of exposure time to ambient air for HSE without functionalization (a), lithium interface resistance as a function of time for in dependency of silane functionalization (b), voltage over time for stripping plating of HSE with 1 vol.-% functionalized and non-functionalized LPS at 0.1 mA cm^{-2} and 80 °C (c), specific ionic conductivity of HSE as well as of pure filler particles as function of the type of thiophosphate filler (a = amorphous, c = crystalline) at 20 °C measuring temperature and a filler content of 1 vol.-% (d).

use of submicron particles was not observed. Overall, the highest ionic conductivity was obtained with 1 vol.-% micron argyrodite filler particles.

As described above for the submicron LPS, an increase in filler content up to 2.5 vol.-% did not further improve the HSE ionic conductivity, likely due to the difficulty of reaching a homogeneous distribution of the LPS submicron particles. Hence, the risk of filler particle agglomeration at 2.5 vol.-% is attempted to be lower for the argyrodite material with an x_{50} of 3 μm. Therefore, the effect of an increased filler content was investigated for the argyrodite material. This was compared to the LPS HSE and a HSE with a passive SiO_2 filler as illustrated in Figure 7.

With rising filler content the conductivity is decreasing for the LPS without functionalization as described above (Figure 2). The comparison of functionalized passive and active filler particles shows that the addition of passive filler particles does not enhance the conductivity. Hence, an improvement in ionic

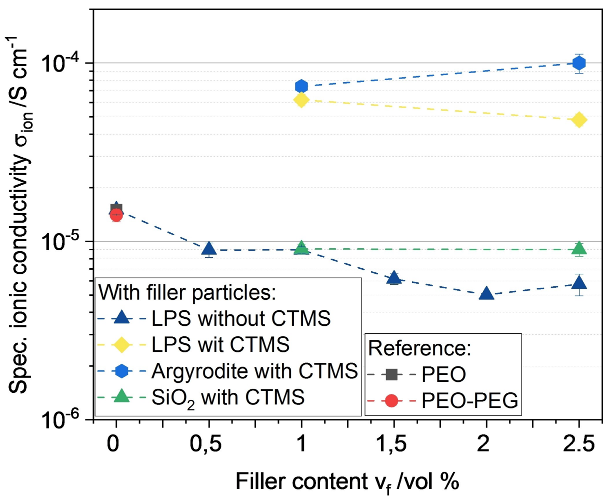

Figure 7. Ionic conductivity in dependency of the filler content for different active fillers (LPS with and without functionalization and argyrodite) as well as passive filler particles (SiO_2 with functionalization). All measurements were conducted at 20 °C.

Research Article
doi.org/10.1002/celc.202300310
Chemistry Europe
European Chemical Societies Publishing

conductivity due to silane (CTMS) induced changes in the polymer structure or suppressed interface effects in between PEO and PEG, as visible in the above shown SEM images can be excluded. In contrast, the ionic conductivity increases with rising filler content up to 0.1 $mS\,cm^{-1}$ for the HSE with the argyrodite filler. However, for higher filler contents of 2.5 vol.-% the ionic conductivity decreased for the submicron LPS. For functionalized submicron LPS SEM images of 1 and 2.5 vol.-% are provided in Figure S3, Supporting Information, showing the increased agglomeration of LPS particles at 2.5 vol.-%. The used process route could not homogenise the HSE sufficiently at amounts as low as 2.5 vol.-% filler, emphasizing the importance of the filler particle size and its behaviour within the hybrid electrolyte. Adjustments in the process could enable a further increase in ionic conductivity at higher filler contents, even for submicron particles. Besides, higher filler particle contents for the micron argyrodite filler particles should be investigated to study whether a further increase in filler content could increase the ionic conductivity even more.

Oxidic filler particles

To investigate the potential transfer of silane functionalization to oxide filler particles, we compared functionalized LATP to non-functionalized LATP as well as functionalized SiO_2 as passive filler material. Additionally, we examined and characterized various filler contents of the functionalized LATP via EIS.

To verify the functionalization of the LATP particles, Fourier transform infrared spectroscopy (FTIR) and TGA measurements were conducted. Next to that, the reaction mechanism is depicted in Figure 8.

While pristine LATP does not schow a significant mass loss, a decrease in mass of 6.14% is detected for funcitonalized LATP particles. Due to multiple washing of the LATP particles in Isopropanol (IPA) no residual silane is expected in the sample leading to the assumption of a covalent bonding of CTMS onto the particle surface. Hence, the TGA data indicates a succesful grafting of the LATP particles. The FTIR analysis of pristine and functionalized LATP particles shows the O–P–O asymmetric bending vibration with overlapping Ti–O stretching vibration at 500 to 600 cm^{-1}[31] and the symmetric stretching vibration of P–O bonding at 800 to 1200 cm^{-1}[32]. For the functionalized LATP particles a shift in the symmetric stretching vibration of P–O bonds at 800 to 1200 cm^{-1} from 927 cm^{-1} to 980 cm^{-1} is visible which is likely attributed to a new peak at 980 cm^{-1} assigned to a Si–O bond additionally confirming the successful grafting of LATP particles with CTMS.[33] A chemical bond in between the CTMS and PEO or PEG is likely as shown by Pan et al., but could not be detected as just a small amount of PEO reacts with the silane and a small shift in the Si–C peak could not be resolved for the FTIR analysis of the HSE (Figure S4,

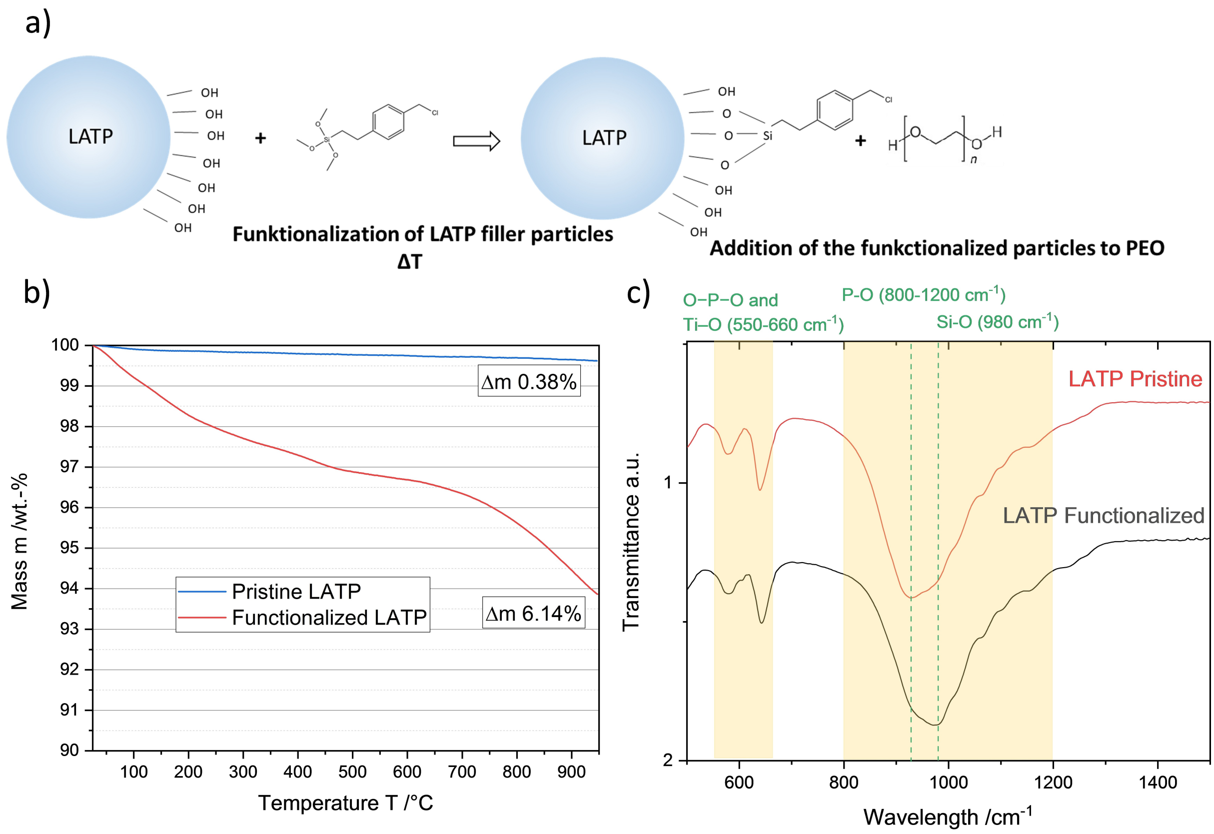

Figure 8. Reaction principle of the functionalization of LATP with CTMS and the addition of the particles to PEO (a), TGA analysis of pristine and functionalized LATP particles (b) and FTIR data of pristine and functionalized LATP particles (c).

Chemistry Europe
European Chemical Societies Publishing

Supporting Information).[23] However, the polarity and hence compatibility of the LATP particles with the polymer is changed.

As already observed for thiophosphate filler particles, the addition of non-functionalized LATP did not improve the ionic conductivity of the HSE (Figure 9). Since the LATP is not sintered in the HSE, high resistances in between the LATP particles are to be expected.[34] The non-functionalized LATP particles form particle clusters, leading to an inhomogeneous LATP distribution (Figure 10a) and the pathways through the LATP clusters do not provide faster ionic transport. The chemical bonding between the polymer and the active filler particles through silanization, on the other hand, leads to an increase in ionic conductivity of the HSE. The highest ionic conductivity is obtained at 10 vol.-% with 0.048 $mS\,cm^{-1}$. For functionalized LATP, a further increase in ionic conductivity with rising filler material content was expected until LATP-LATP contacts occur. But as discussed for the thiophosphate filler particles, the occurrence of filler particle contacts is also dependent on the particle size and dispersion degree. For functionalized LATP filler particles with a particle size of x_{50} of 0.085 μm, a sufficient homogenization was reached up to 10 vol.-% as depicted in SEM images of the cross-section in Figure 10b.

To investigate whether active filler particles are necessary to obtain increased lithium ion conductivity, 10 vol.-% passive filler material was functionalized and added to the HSE. At 20 °C measurement temperature, a slight increase in ionic conductivity from 0.014 to 0.026 $mS\,cm^{-1}$ was observed. However, as shown in Figure 9b, the use of functionalized active filler particles leads to a significantly greater improvement in the ionic conductivity of the HSE. In addition, a transference number of 0.576 was determined for the HSE with functionalised LATP in contrast to 0.52 for the PEO-PEG-PSE, which supports the hypothesis that the active filler particles are participating in lithium ion transport. To clarify for the HSE with functionalized LATP whether the lithium ion transport occurs

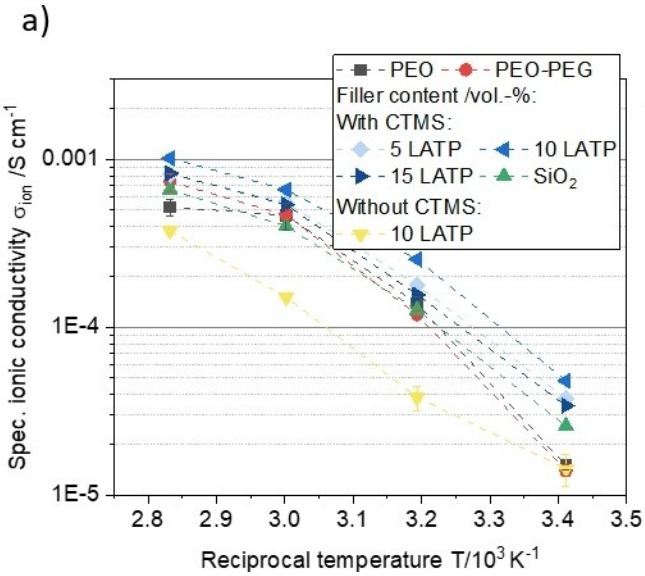

Figure 9. Ionic conductivity of PSE and HSE with different LATP content and with silane functionalization in dependence of the measuring temperature (a), ionic conductivity in dependence of the filler content and functionalization at 20 °C measuring temperature (b).

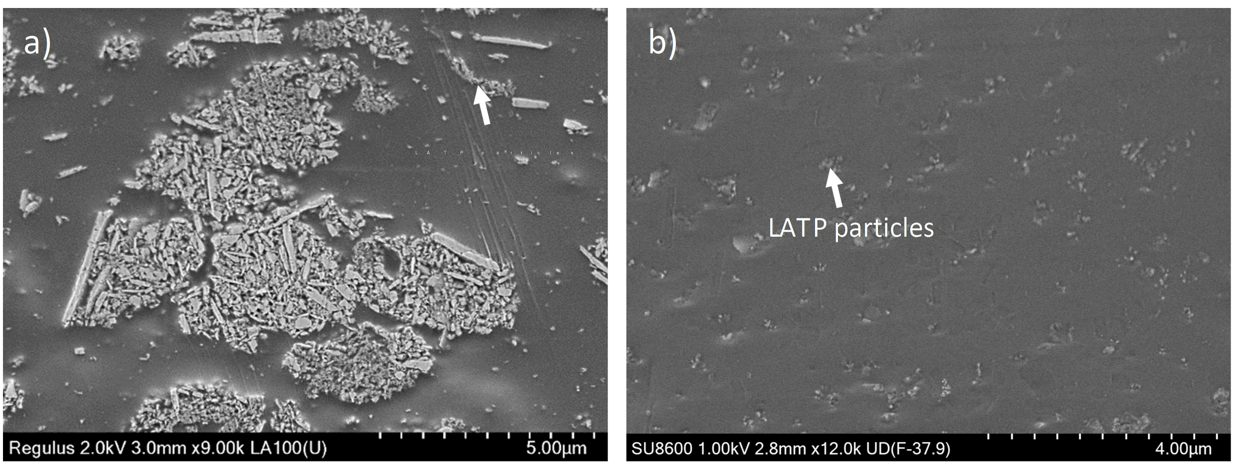

Figure 10. SEM images of HSE with 10 vol.-% LATP (a) and HSE with 10 vol.-% LATP with silane functionalization (b).

along the filler particles interface or through the particle bulk, the LATP particle size was varied.

Therefore, the LATP particles were ground by wet media milling to reach various particle sizes. In order to study the structural changes during grinding, X-ray diffraction measurements were conducted. As described in Yoon et al. and Liu et al., a reduction of both crystallite size and crystallinity of the LATP particles leads to decreasing peak intensity.[35,36] As visible in the XRD measurements, a decrease in peak intensity is observed with rising grinding speed and, thus, stress intensity (Figure S7, Supporting Information). Hence, dependent on the grinding conditions not only the filler particle size, but also the crystallinity and grain size is changed. Due to the structural changes of the LATP particles it is not possible to consider only a correlation between ionic conductivity and particle size. In addition, the crystallite size determined by XRD measurements, must also be considered. Therefore, for a filler content of 10 vol.-% the ionic conductivity is shown in dependency of the crystallite size Figure 11a for two different particle size ranges. Besides, the ionic conductivity is presented as a function of both particle size and crystallite size (Figure 11b).

For a similar LATP particle size, the ionic conductivity decreases with a reduced crystallite size. For the particle size range of 0.085 to 0.14 μm with rising crystallite size an ionic conductivity of 0.026 to 0.048 $mS\,cm^{-1}$ is reached. This indicates a strong influence of the LATP particle structure on the ionic transport in the HSE. As depicted in Figure 11b, the described effect of the structural changes of the LATP particles is visible with an increase in conductivity for LATP particles with similar particle size, but rising crystallite size. In addition, a reduced LATP particle size leads to an increase in ionic conductivity from 0.035 $mS\,cm^{-1}$ to 0.056 $mS\,cm^{-1}$ for an x_{50} of 1.69 μm and 0.78 μm, respectively. With a further reduction of the LATP particle size to a x_{50} of 0.1 μm stronger structural changes occur and an ionic conductivity of 0.026 $mS\,cm^{-1}$ was obtained. The surface conductivity of the LATP particles therefore influences the HSE ionic conductivity, indicating that the LATP particle surface participates in the lithium ion transport. This effect reveals that an adapted filler particle design with a high

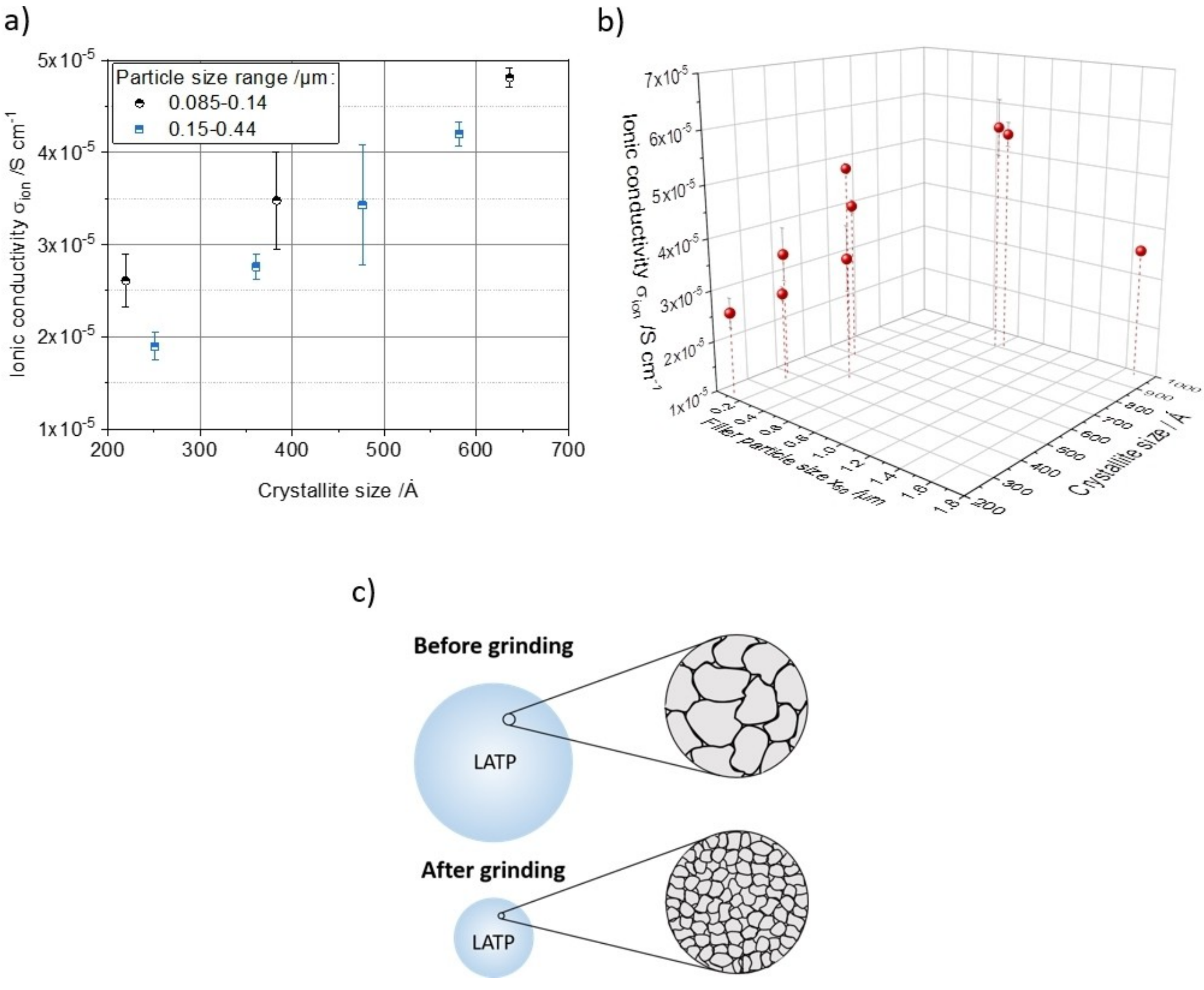

Figure 11. Ionic conductivity of HSE PEO-PEG with 10 vol.-% functionalized LATP at RT in dependency of the crystallite size for different measured particle size ranges (a) and ionic conductivity in dependence of the particle size and maximum XRD peak intensity (b), scheme of particle surface before and after grinding with different crystallite sizes (c).

crystallinity and crystallite size at the surface is necessary in contrast to applications for pure oxide SE where crystallinity and grain size is increased by a final sintering step.[37,38] A clear effect of the particle size can only be studied if the filler particles show the same structural properties. Due to the stress applied during grinding, these changes cannot be avoided. A slight reduction in particle size of the LATP enhances the performance and thus, the grinding should take place at comparably mild conditions e.g. low rotational speeds before the amorphisation shows a negative effect. The higher the speed, the higher the intensity of stressing and the number of stressing events. It is worth noting, that the particle size reduction occurs immediately at all speeds. However, at low speeds the crystallite size is only reduced after sufficient time and therefore number of stressing events, allowing to reduce the particle size at mild conditions without excessive alteration of the crystallites (Figure S8, Supporting information).

Nonetheless, given sufficient homogenization, further studies should be conducted to investigate in more detail, if a further reduction in filler particle size with minimal structural changes of the filler particles can increase the ionic conductivity further.

Conclusions

In this work, different types of oxide and thiophosphate filler particles were investigated as active filler particles for polymer electrolyte based hybrid solid electrolytes. First, a suitable process route was chosen, based on studies on the influence of the stress intensity and process time during dispersion. With rising stress intensity, the HSE porosity decreased and an improved ionic conductivity was observed as the LPS particles as well as the LiTFSI were distributed more homogeneously in the polymer matrix. Therefore, the use of a dissolver or a more intense dispersing process, such as kneading, is highly recommended for the dispersing step.[39] Next to that, the time needed for ligand formation of the suspension was found to be an important consideration.

Furthermore, no improvement in ionic conductivity could be obtained for oxide and thiophosphate filler particles if no functionalization was applied. For non-functionalized thiophosphate filler particles, the precipitation of sulfur was detected to hinder the ionic transport. Through successful silanization verified by TGA measurements the stability of the suspension could be significantly improved. Besides the porosity of the HSE, as well as filler particle distribution could be improved resulting in an increase in ionic conductivity. Through functionalization of the LPS particles the stability under ambient conditions, i.e. moist air, as well as the chemical stability against lithium, were improved. The incorporation of filler particles with different intrinsic ionic conductivities revealed a direct influence of the filler particle intrinsic conductivity on the HSE ionic conductivity. Besides, the particle size showed a great influence on filler content at which agglomeration started, emphasizing the importance of further investigations of the dispersion step for incorporation of submicron filler particles.

Likewise, for oxide filler particles the silane functionalization through Si–O bond on the LATP surface showed a significant improvement in ionic conductivity of the HSE. In addition, a strong interaction of grinding-induced structural changes and filler particle size with the resulting ionic conductivity of the HSE was detected. The results indicate that the surface of the filler particles participates in the lithium ion transport. The presented results illustrate the interdependence of particle size-induced challenges in achieving sufficient filler particle homogenisation along with structural differences due to different grinding energies and intensities. Finally, the importance of surface properties of filler particles on the overall HSE ionic conductivity highlights the requirement for an adapted filler design specifically tailored for HSE applications.

Experimental Section

Materials and experimental methods

Initially, all used materials were dried under vacuum (25 mbar) at 40 °C for 4 h. For the solid polymer electrolyte manufacturing polyethylene oxide (Mw = 900,000 g/mol) (Dow) as well as optional polyethylene glycol (Mw = 2,000 g/mol) (Sigma-Aldrich) with the lithium salt bis(trifluoromethane)sulfonimide (LiTFSI) (Clariant) was used in a molar ratio of Li^+/O 1:14. Various filler particles were added, each with different material properties as shown in the table below.

The filler content was varied between 0.5 and 2.5 vol.-% for the thiophosphate filler particles and between 5 and 15 vol.-% for the oxide filler particles.

Thiophosphate hybrid HSE

The thiophosphate filler particles were dispersed in acetonitrile (ACN) in a glovebox under argon atmosphere. A rest step of the suspension of 0 to 24 h prior to the subsequent dissolving step was applied. For further processing the suspension was transferred to a dry room (dew point −45 °C at 20 °C ambient temperature). For hybrid solid electrolytes (HSE), silane, (Chloromethyl)(Phenylethyl)Trimethoxysilane (CTMS) was added to the ACN-thiophosphate filler suspension and stirred using a magnetic stirrer at 60 °C for 1 h. Afterwards, the polymer (PEO:PEG with a ratio of 80:20 wt.%) and LiTFSI were added to the suspension and homogenized in a dissolver (DISPERMAT LC, VMA-Getzmann GmbH, Germany) using a 40 mm toothed disc. Initially, a rotational speed of 2000 rpm was applied and after 5 min the rotational speed was increased to 5000 rpm for 25 min. For a PEO-PEG-LiTFSI PSE with 1 vol.-% LPS the influence of the energy input in the dispersing step was investigated. Therefore, in addition to the dissolver a magnetic stirrer and shaking plate were used to dissolve and disperse the PEO, PEG, LiTFSI and LPS. Afterwards the solution was coated directly or after a rest time of 24 h by an applicator with a doctor blade (ZAA 2300, Zehntner Testing Instruments, Switzerland) at a heat plate temperature of 30 °C and a speed of 5 mm s^{-1} onto a non-stick release foil. In order to fabricate separator sheets with a sufficient thickness for handling of approx. 80 μm, three layers were coated on top of each other with a drying time of 10 min each. Finally, the applicator was heated to 80 °C to fuse the individual separator layers.

Oxide hybrid HSE

For the oxide-based HSEs, the influence of a pre-grinding step of the LATP filler particles was evaluated and compared to the pristine LATP particles. For both options, the LATP particles (SCHOTT AG, Germany) were dispersed in isopropanol (IPA). The grinding was performed in a planetary ball mill (PULVERISETTE 7, FRITSCH GmbH, Germany) with an 80 ml grinding bowl volume using ZrO2 grinding media with a diameter of 1 mm and a solids content of 20 wt.-% LATP in IPA. The grinding time was set to 25 min with a rotational speed of 400 rpm. Besides, for the variation of the LATP particle size different grinding conditions were applied. The grinding time was varied between 2 and 60 min for three different rotational speeds with 200, 400 and 600 rpm and a solids content of 10 wt.-%. For further processing, the suspension was transferred to a dry room (dew point −45 °C at 20 °C ambient temperature). For the HSEs containing silane, CTMS was added to the suspension which was stirred for 1 h at 60 °C with a magnetic stirrer. For further processing ACN, the polymer (PEO:PEG 80:20 wt.-%) and LiTFSI was added and dissolved (DISPERMAT LC, VMA-Getzmann GmbH, Germany) using a 40 mm toothed disc. A rotational speed of 2000 rpm was applied in the beginning and after 5 min the rotational speed was increased to 5000 rpm for 25 min. The coating was performed with the above mentioned process parameters as for the thiophosphate HSEs.

Characterization

The porosity of the fabricated separator films was calculated based on the theoretical ρ_{theo} and the measured density ρ_{real} with the separator mass *m*, the sample volume *V*, the raw density ρ_i and weight content x_i of the single components:

$$\varepsilon = 1 - \frac{\rho_{real}}{\rho_{theo}} \text{ with } \rho_{real} = \frac{m}{V}\ ;\ \rho_{theo} = \frac{1}{\sum_{i=1}^{n} \frac{x_i}{\rho_i}} \tag{1}$$

In order to determine the H_2S content released from the hybrid electrolyte, release tests were carried out under normal and dry room atmosphere for the separator films with 1 vol.-% LPS with and without CTMS. For this purpose, 1 g of the sample was placed in a desiccator and the hydrogen sulfide content was determined manually over 90 min with a H_2S sensor X-am 5000 (Dräger, Germany). To ensure a homogeneous distribution of the air, a ventilator was placed in the desiccator. Using the sample mass of 1 g and the volume of 18,500 ml, the amount of H_2S released can be determined in $cm^3\ g^{-1}$.

Raman spectroscopy (XR 2 Raman Microscope, Thermo Scientific, USA) was used to determine the composition of precipitated material in the suspension. Therefore, the material was applied to an object slide and sealed airtight. The measurement was carried out with a wavelength of 532 nm and 1 mW. Each measurement was conducted three times with 60 seconds exposure time.

To verify the functionalization thermogravimetric analysis (TGA) of functionalized and pristine LATP and LPS particles was performed, with a heating rate of 10 K/min in a temperature range of 25 to 950 °C in nitrogen atmosphere (TGA/DSC 1 sTARe; Mettler-Toledo GmbH, Greifensee, Switzerland). The chemical bonds of pristine and functionalized LATP particles as well as PSE and HSE were analyzed via Fourier Transform Infrared Spectroscopy (FTIR, VERTEX 70, Bruker). Three washing steps with IPA for LATP and heptane for LPS were applied, in order to remove residual silane that was not bonded to the particle surface before analyzing via TGA and FTIR.

The ionic resistance was measured via potentiostatic electrochemical impedance spectroscopy (EIS) (ZENNIUM, Zahner, Germany) as described in Wiegmann and Helmers et al. using blocking conditions and varied measurement temperature of 20 to 80 °C.[44] The resulting Nyquist plot and equivalent circuit are depicted for the pure PSE and different HSE types in Figure S10 and Figure S11, Supporting Information. The specific ionic conductivity was calculated using the following equation with the ionic resistance R_{ion}, the separator thickness δ and the electrochemically active area A.

$$\sigma_{ion} = \frac{\delta}{R_{ion} \cdot A} \tag{2}$$

The stability of the separator against lithium was investigated in copper-lithium-separator-lithium-copper coin cells by measurement of the interface resistance in dependency of storage time via EIS. The cells were heated to 80 °C once to ensure a sufficient contact between the lithium foil and the separator. The resistance was measured at regular intervals over a period of one month at a measuring temperature of 20 °C. The cycling of symmetric lithium cells was performed at 0.1 $mA\,cm^{-2}$ with 1 h for each stripping and plating and 80 °C measuring temperature. The transference number was determined in symmetric lithium cells via Bruce-Vincent method by combined EIS measurements and DC polarization with 10 mV.[45]

Cross sections of the separator films were prepared using the Broad-Ion-Beam (BIB) technology with the IM5000 "ArBlade". Subsequently, scanning electron microscope (SEM) (SU5000, Hitachi High Tech) images of the cross section were recorded to analyze the filler particle distribution.

To determine the crystallite size of the LATP particles X-ray diffraction (XRD) (Empyrean, Panalytical) measurements were performed with a Cu-K_α radiation, wavelength λ of 0.154 nm, in a range of 2θ from 20 to 90° and a step size of 0.053°. The XRD data was analyzed via the Williamson-Hall method using the Highscore Plus software to determine the crystallite size.

Supporting Information

The authors have cited additional references within the Supporting Information.[46–48]

Acknowledgements

The authors gratefully acknowledge the financial support by the federal ministry of education and research (BMBF) giving the base for the here demonstrated results within the research project 3D-SSB (funding number 3XP0202F) and FB2-Prod (funding number 03XP0432 A). They would also like to thank Jeroen Volbeda, Eike Wiegmann and Jessica Gerstenberg for the helpful discussions. Open Access funding enabled and organized by Projekt DEAL.

Conflict of Interests

The authors declare no conflict of interest.

Data Availability Statement

The data that support the findings of this study are available from the corresponding author upon reasonable request.

Keywords: all-solid-state battery · composite solid electrolytes · functionalization of filler particles · hybrid solid electrolyte · polymer solid electrolyte

[1] L. Lu, X. Han, J. Li, J. Hua, M. Ouyang, *J. Power Sources* **2013**, *226*, 272.
[2] A. Manthiram, X. Yu, S. Wang, *Nat. Rev. Mater.* **2017**, *2*, 1.
[3] Y. J. Nam, D. Y. Oh, S. H. Jung, Y. S. Jung, *J. Power Sources* **2018**, *375*, 93.
[4] T. Winie, *Polymer Electrolytes. Characterization and Applications*, John Wiley & Sons Incorporated, Newark, **2020**.
[5] C. Vincent, B. Scrosati, *Modern Batteries*, Elsevier, **1997**.
[6] Hekselman, M. Kalita, A. Plewa-Marczewska, G. Z. Żukowska, E. Sasim, W. Wieczorek, M. Siekierski, *Electrochim. Acta* **2010**, *55*, 1298.
[7] H. Zhang, C. Liu, L. Zheng, F. Xu, W. Feng, H. Li, X. Huang, M. Armand, J. Nie, Z. Zhou, *Electrochim. Acta* **2014**, *133*, 529.
[8] A. Junji, K. Norihito, H. Hiroshi, *J. Solid State Chem.* **2009**, *182*, 2046.
[9] R. Murugan, V. Thangadurai, W. Weppner, *Angew. Chem. Int. Ed.* **2007**, *46*, 7778.
[10] A. Gurung, J. Pokharel, A. Baniya, R. Pathak, K. Chen, B. Sagar Lamsal, N. Ghimire, W. Zhang, Y. Zhou, Q. Qiao, *Sustain. Energy Fuels* **2019**, *3*, 3279.
[11] T. Krauskopf, H. Hartmann, W. Zeier, J. Janek, *ACS Appl. Mater. Interfaces* **2019**, *11*, 14463.
[12] R. F. Samsinger, M. Letz, J. Schuhmacher, M. Schneider, A. Roters, D. Kienemund, H. Maune, A. Kwade, *J. Electrochem. Soc.* **2020**, *167*, 140510.
[13] C. Yang, K. Fu, Y. Zhang, E. Hitz, L. Hu, *Advanced materials (Deerfield Beach, Fla.)* **2017**, *29*.
[14] Y. Kato, S. Hori, T. Saito, K. Suzuki, M. Hirayama, A. Mitsui, M. Yonemura, H. Iba, R. Kanno, *Nat. Energy* **2016**, *1*, 1.
[15] J.-M. Doux, Y. Yang, D. H. S. Tan, H. Nguyen, E. A. Wu, X. Wang, A. Banerjee, Y. S. Meng, *J. Mater. Chem. A* **2020**, *8*, 5049.
[16] K. Kerman, A. Luntz, V. Viswanathan, Y. Chiang, Z. Chen, *J. Electrochem. Soc.* **2017**, *164*, A1731.
[17] X. Xu, G. Hou, X. Nie, Q. Ai, Y. Liu, J. Feng, L. Zhang, P. Si, S. Guo, L. Ci, *J. Power Sources* **2018**, *400*, 212.
[18] C. Wang, X.-W. Zhang, A. J. Appleby, *J. Electrochem. Soc.* **2005**, *152*, A205.
[19] S. Chen, J. Wang, Z. Zhang, L. Wu, L. Yao, Z. Wei, Y. Deng, D. Xie, X. Yao, X. Xu, *J. Power Sources* **2018**, *387*, 72.
[20] X. Li, D. Wang, H. Wang, H. Yan, Z. Gong, Y. Yang, *ACS Appl. Mater. Interfaces* **2019**, *11*, 22745.
[21] H. Huo, N. Zhao, J. Sun, F. Du, Y. Li, X. Guo, *J. Power Sources* **2017**, *372*, 1.
[22] J. Lee, T. Howell, M. Rottmayer, J. Boeckl, H. Huang, *J. Electrochem. Soc.* **2019**, *166*, A416–A422.
[23] K. Pan, L. Zhang, W. Qian, X. Wu, K. Dong, H. Zhang, S. Zhang, *Advanced materials (Deerfield Beach, Fla.)* **2020**, *32*, e2000399.
[24] J. Xu, J. Li, Y. Li, M. Yang, L. Chen, H. Li, F. Wu, *Advanced materials (Deerfield Beach, Fla.)* **2022**, *34*, e2203281.
[25] A. Kwade, M. Möller, J. Müller, J. Hesselbach, S. Zellmer, S. Doose, J. Mayer, P. Michalowski, M. Powell, S. Breitung-Faes, *Kona* **2023**, *40*, 50.
[26] R. W. Gomez, J. L. Perez, V. Marquina, R. Ridaura, M. L. Marquina, *Rev. Mex. Fis.* **2007**, *53*.
[27] A. Zarinwall, T. Waniek, R. Saadat, U. Braun, H. Sturm, G. Garnweitner, *Langmuir* **2021**, *37*, 171.
[28] L. M. Corredor, M. M. Husein, B. B. Maini, *Ind. Eng. Chem. Res.* **2019**, *58*, 9888.
[29] H. Stöffler, T. Zinkevich, M. Yavuz, A.-L. Hansen, M. Knapp, J. Bednarčík, S. Randau, F. H. Richter, J. Janek, H. Ehrenberg et al., *J. Phys. Chem. C* **2019**, *123*, 10280.
[30] F. Croce, L. Persi, B. Scrosati, F. Serraino-Fiory, E. Plichta, M. A. Hendrickson, *Electrochim. Acta* **2001**, *46*, 2457.
[31] J. Li, C. Liu, C. Miao, Z. Kou, W. Xiao, *Ionics* **2022**, *28*, 63.
[32] Y. Huang, Y. Jiang, Y. Zhou, Z. Hu, X. Zhu, *ChemElectroChem* **2019**, *6*, 6016.
[33] L. Wang, G. Xie, X. Mi, B. Zhang, Y. Du, Q. Zhu, Z. Yu, *ACS Omega* **2023**, *8*, 20116.
[34] H. Yamada, D. Tsunoe, S. Shiraishi, G. Isomichi, *J. Phys. Chem. C* **2015**, *119*, 5412.
[35] J. Liu, T. Liu, Y. Pu, M. Guan, Z. Tang, F. Ding, Z. Xu, Y. Li, *RSC Adv.* **2017**, *7*, 46545.
[36] Y. Yoon, J. Kim, C. Park, D. Shin, *JCPR* **2013**, *14*.
[37] L. K. Suk-Joong, *Sintering. Densification, grain growth, and microstructure*, Elsevier Butterworth-Heinemann, Amsterdam, Boston, London, **2005**.
[38] H. Morimoto, M. Hirukawa, A. Matsumoto, T. Kurahayashi, N. Ito, S.-i. Tobishima, *Electrochemistry* **2014**, *82*, 870.
[39] R. F. Samsinger, S. O. Schopf, J. Schuhmacher, P. Treis, M. Schneider, A. Roters, A. Kwade, *J. Electrochem. Soc.* **2020**, *167*, 120538.
[40] P. Mirmira, J. Zheng, P. Ma, C. V. Amanchukwu, *J. Mater. Chem. A* **2021**, *9*, 19637.
[41] M. Hofer, M. Grube, C. F. Burmeister, P. Michalowski, S. Zellmer, A. Kwade, *Adv. Powder Technol.* **2023**, *34*, 104004.
[42] M. Batzer, K. Voges, W. Wang, P. Michalowski, A. Kwade, *Materials Today Communications* **2022**, *30*, 103189.
[43] L. Froboese, J. van der Sichel, T. Loellhoeffel, L. Helmers, A. Kwade, *J. Electrochem. Soc.* **2019**, *166*, A318.
[44] E. Wiegmann, L. Helmers, P. Michalowski, A. Kwade, *Adv. Ind. Manuf. Eng.* **2021**, *3*, 100065.
[45] P. Bruce, *Solid State Ionics* **1988**, *28–30*, 918.
[46] A. A. Issa, A. S. Luyt, *Polymer* **2019**, *11*.
[47] Y.-S. Li, A. Ba, *SAA* **2008**, *70*, 1013.
[48] N. S. Vrandečić, M. Erceg, M. Jakić, I. Klarić, *Thermochim. Acta* **2010**, *498*, 71.

Manuscript received: August 21, 2023
Revised manuscript received: September 14, 2023
Version of record online: October 18, 2023